International Journal of Hydrogen Energy 59 (2024) 570–581

Contents lists available at ScienceDirect

International Journal of Hydrogen Energy

journal homepage: www.elsevier.com/locate/he

Performance assessment of a 25 kW solid oxide cell module for hydrogen production and power generation

Diana M. Amaya Dueñas *, Dirk Ullmer, Marc Riedel, Santiago Salas Ventura, Matthias Metten, Marius Tomberg, Marc P. Heddrich, S. Asif Ansar

German Aerospace Center (DLR), Institute of Engineering Thermodynamics, Pfaffenwaldring 38-40, 70569, Stuttgart, Germany

ARTICLE INFO

Handling Editor: Fanglin F. Chen

Keywords:
Hydrogen polygeneration
High Temperature Electrolysis (HTE)
Solid Oxide Fuel Cell (SOFC)
Solid Oxide Electrolysis (SOEL)
Reversible Solid Oxide Cell (rSOC)
Area Specific Resistance (ASR)

ABSTRACT

Hydrogen produced via water electrolysis from renewable electricity is considered a key energy carrier to defossilize hard-to-electrify sectors. Solid oxide cells (SOC) based reactors can supply hydrogen not only in electrolysis but also in fuel cell mode, when operating with (synthetic) natural gas or biogas at low conversion (polygeneration mode). However, the scale-up of SOC reactors to the multi-MW scale is still a research topic. Strategies for transient operation depending on electricity intermittency still need to be developed. In this work, a unique testing environment for SOC reactors allows reversible operation, demonstrating the successful switching between electrolysis (−75 kW) and polygeneration (25 kW) modes. Transient and steady state experiments show promising performance, with a net hydrogen production of 53 kg day^{-1} in SOEL operation with ca. −75 kW power input. The experimental results validate the scaling approach since the reactor shows homogenous temperature profiles.

1. Introduction

Hydrogen is a key energy carrier for the decarbonization of anthropocentric activities, even more when an energy crisis may threaten the productivity of various industrial sectors. To limit the increment of the average global temperature to 1.5 °C, a vast transformation of the energy sector in terms energy production, consumption and transport is urgently needed [1]. The European Union's Hydrogen Strategy aims at using hydrogen as energy vehicle for power generation and storage for a wide range of industrial, transport, mobility and building applications [2–4]. A pathway for hydrogen production is electrolysis via electric power from renewable energy sources (RES), such as wind power or photovoltaic systems. However, the intermittent nature of RES raises challenges to the stability of the electrical grid. Namely, the rapid increase on demand for hydrogen as energy carrier and storage medium, to accommodate the supply and demand fluctuation in the grid, represents the urgent need to scale-up the hydrogen production from RES.

Industrial end-users require a secure and uninterrupted supply of hydrogen, independent of the intermittent RES. An electrolyzer unit that could meet a continuous hydrogen production, is a solid oxide cell (SOC) reactor-module that consists of multiple stacks with numerous cells.

Promising results at different scales, i.e. at cell and stack level, have contributed to the scale-up of SOC-systems up to the kW-level during the last decade, by implementing different SOC architectures in relevant operating conditions [5,6]. However, experimental data in reversible operation of SOC-modules, especially at higher kW-levels, are scarce [7–15]. Most of the research reported so far has focused on short stacks [16–25] with up to 10 repeating cells, referred to as repeating units (RUs).

The EU project "SWITCH" aims to develop a prototype that supplies green hydrogen from renewable electricity (via high temperature electrolysis), as well as from natural gas or biogas (via reforming reactions), while producing electrical power. The main objective of SWITCH is to implement and demonstrate a polygeneration system that secures continuous and renewable hydrogen production. The core of such a system is a reversible SOC module based on fuel-electrode-supported cells with an advanced fuel processing unit able to manage both: steam generation and methane reactions. Preliminary investigations on a stack with 70 repeating units (RUs) have already shown promising results within SWITCH [26].

In the frame of SWITCH, this work focuses on the demonstration of a reversible SOC module (25 kW SOFC/75 kW SOEL). SOEL operation at thermoneutral voltage U_{th} is investigated in steady state operation, which corresponds to ~1.29 V per cell (for adiabatic operation) for high

* Corresponding author.
E-mail addresses: Diana.AmayaDuenas@dlr.de (D.M. Amaya Dueñas), Matthias.Metten@dlr.de (M. Metten).

https://doi.org/10.1016/j.ijhydene.2024.01.346
Received 21 November 2023; Received in revised form 22 January 2024; Accepted 29 January 2024
Available online 9 February 2024

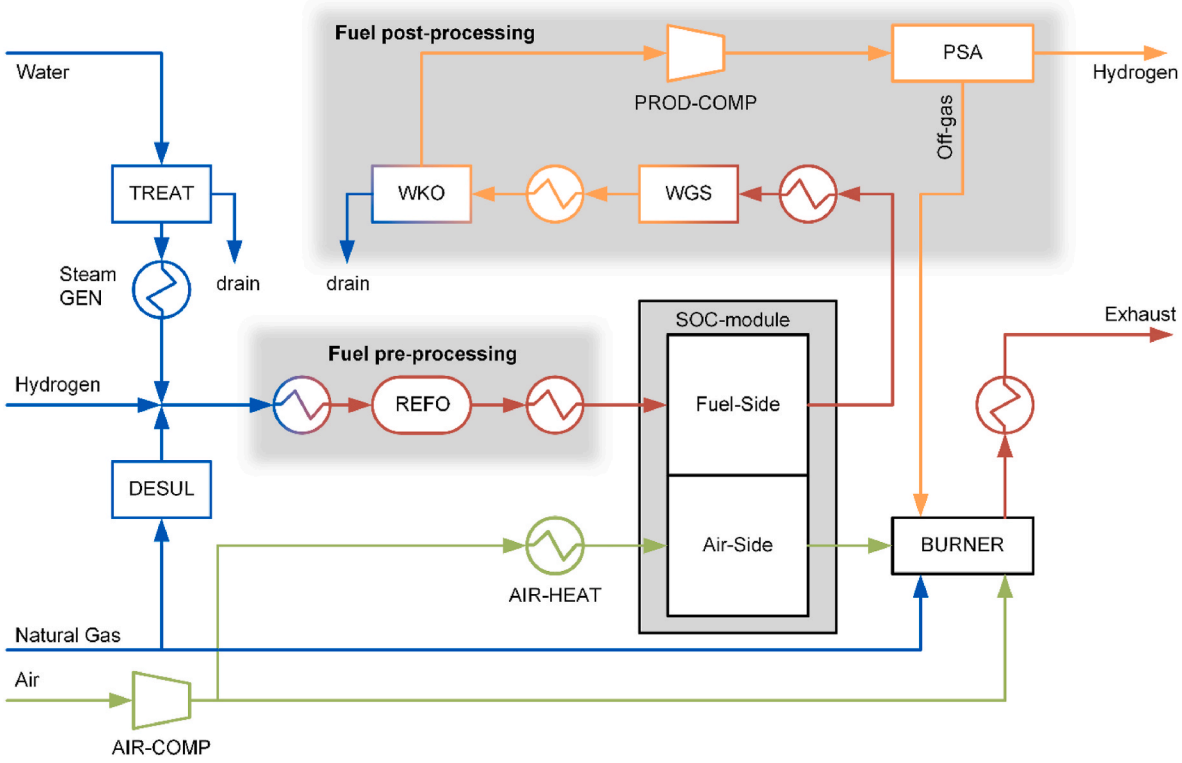

Fig. 1. Schematic PFD of the SWITCH-system: TREAT: Water treatment unit; Steam GEN: steam generator; DESUL: desulphurization unit, AIR-COMP: Air Compressor; REFO: pre-Reformer; AIR-HEAT: Air Heater; WGS: Water-Gas-Shift reactor; WKO: water knock-out; PROD-COMP: product compressor; PSA: pressure swing adsorption.

temperature steam electrolysis. At this voltage, the cooling from the endothermic electrolysis reaction is balanced by the Joule-heat originated from the resistances of the cells [5]. This operation mode is in principle denoted as isothermal operation because the difference between the inlet and outlet temperatures of the cells is negligible, minimizing local thermal gradients and thermomechanical stresses [27,28]. However, when operating stack-modules external heat losses need to be compensated to allow isothermal operation as these are not considered in the adiabatic case. Therefore, such systems operate slightly above the thermoneutral voltage. The main objectives of this investigation are:

(i) to demonstrate reversible operation of a 25 kW SOFC/75 kW SOEL module alternating between SOEL and SOFC operating modes during a switching procedure below 30 min, up to a daily hydrogen production of 50 kg (targeted hydrogen production capacity),
(ii) to develop a performance map of the reactant conversion and the daily net hydrogen production at different temperatures in thermoneutral operation, based on the experimental results in SOEL mode,
(iii) to measure steady state data of polarization curves with a constant reactant conversion rate throughout the endothermic, thermoneutral and exothermic operation aiming at quantifying the area specific resistance (ASR) of the SOC module,
(iv) to identify the benefits and limitations of the ASR estimation between steady state data and electrochemical impedance spectroscopy (EIS).

2. Materials and methods

In this section, the description of the SWITCH system and SOC-reactor, called large stack module (LSM) from SolydEra are presented, as well as the test facility and equipment that were used for the testing and characterization of the LSM.

2.1. Description of SWITCH prototype

The main process flow diagram (PFD) of the SWITCH system is depicted in Fig. 1.

Firstly, Water is purified in the Water Treatment unit (TREAT) and steam is generated in the Steam generator (Steam GEN). Secondly, in electrolysis mode, the steam is mixed with a small amount of hydrogen, and pre-heated to operation temperature of the SOC in the fuel pre-processing part. Within the SOC-module hydrogen is produced via electrolysis and send to the fuel post-processing part. In poly-generation mode, when renewable electricity is not available, natural gas is used. For that it is desulfurized (DESUL), mixed with steam and pre-reformed in the fuel pre-processing part via endothermal steam reforming (SMR – eq. (1)) in the reformer (REFO):

$$CH_4 + H_2O \rightleftharpoons 3H_2 + CO \quad (SMR) \qquad \text{eq. (1)}$$

In the SOC-module, electricity and hydrogen are produced in parallel in poly-generation mode by running in fuel cell mode with a low conversion ratio (c.f. [29]). Afterwards, remaining steam is shifted towards hydrogen within the Water Gas shift reactor (WGS –eq. (2)) with CO from internal steam reforming during the fuel cell reaction.

$$CO + H_2O \rightleftharpoons \quad H_2 + CO_2 \quad (WGS) \qquad \text{eq. (2)}$$

In both modes the produced stream is dried in the Water knock-out (WKO) and compressed (PROD-COMP) for purification in the pressure swing adsorption (PSA) within the Fuel post-processing part.

Air is supplied via the air compressor (AIR-COMP) and heated towards operation temperature of the SOC in AIR-HEAT.

The main overall heat demand during operation, heat-up and cool-down is managed via the BURNER. For that, recycled Off-gas from the PSA and natural gas is used. Heat is recovered internally from the

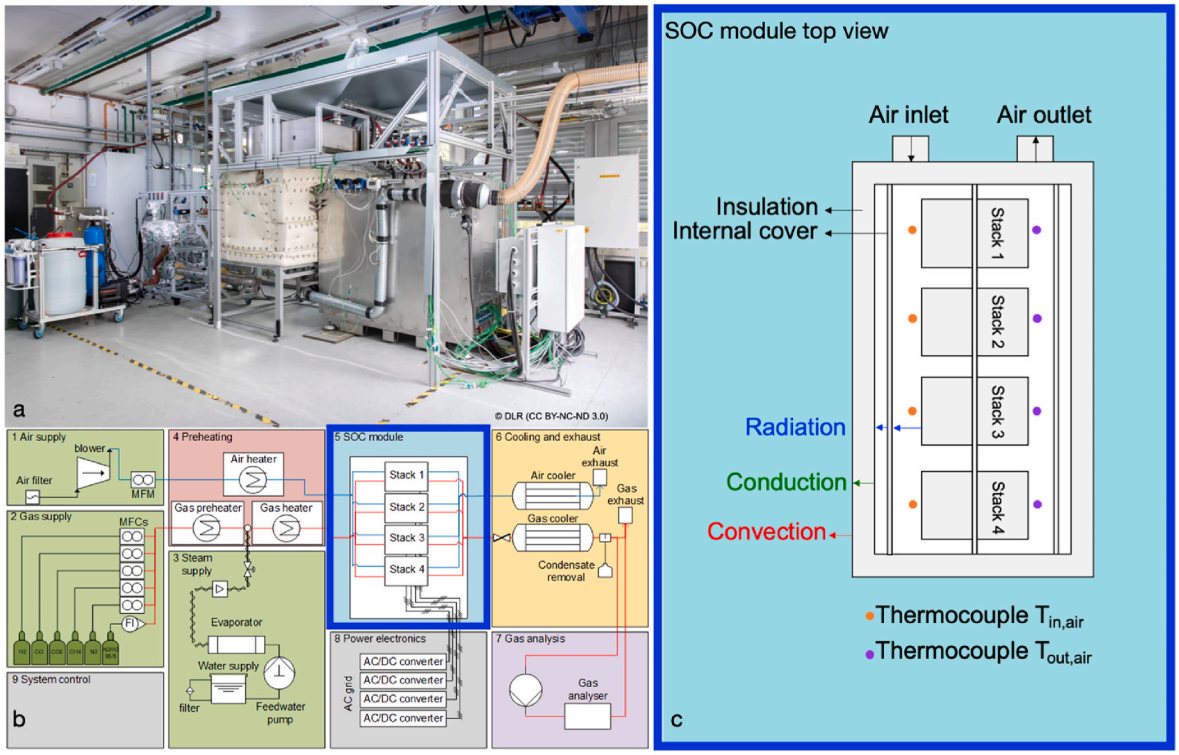

Fig. 2. (a): Test environment "GALACTICA" for the testing of the large stack module (LSM) of SolydEra at the Institute of Engineering Thermodynamics from the German Aerospace Center (DLR) in Stuttgart, Germany. (b): Process flow diagram of the test bench, highlighting its different components of the test environment GALACTICA. (c): Top view of SOC module tested at GALACTICA. An overview of the thermocouples within the module, as well as the different heat transport phenomena are depicted.

exhaust towards the Fuel pre-processing part and to heat-up the Air for the SOC in the heat exchanger AIR-HEAT.

2.2. Large stack module (LSM)

The 25 kW large stack module (LSM) was supplied by SolydEra, which consisted of 4 stacks, with fuel-electrode-supported planar cells [13]. The total active area per RU was of 320 cm^2. At each stack, temperature sensors for the inlet and outlet of air and fuel flows were implemented. Pressure sensors were located inside the air and fuel pipes close to the corresponding flanges. For this work, the LSM was tested on the test facility for SOC reactors from the Institute of Engineering Thermodynamics of the German Aerospace Center (DLR) in Stuttgart, Germany.

2.3. SOC module test facility – experimental setup

The test environment GALACTICA (Fig. 2a) is a large-scale research testing facility at the Institute of Engineering Thermodynamics of the German Aerospace Center (DLR) in Stuttgart. It was built to investigate the technical challenges involved in scaling up SOC-systems and to identify critical operating conditions for the development of control strategies. It offers the unique possibility of investigating large solid oxide cell (SOCs) modules with multiple stacks, while varying operating temperature, fuel composition, and operation modes: either in fuel cell mode as solid oxide fuel cell (SOFC) for power generation (up to 40 kW_{el} output) or in electrolysis mode as solid oxide electrolyzer (SOEL) for hydrogen and/or syngas production (up to 120 kW_{el} input). Reversible operation (rSOC) is also possible by using four bi-directional electric loads. Two air compressors with variable speed supply process air. Gases such as H_2, CO_2, CO, N_2 and CH_4 are available for the fuel gas feed, as well as H_2O steam (28 kg/h). Mixture of these gases allow to emulate pre-reformer compositions at the inlet of the SOC module if needed. From room temperature, GALACTICA supplies the fuel and air streams to the SOC module up to an operating temperature between 650 °C–850 °C with an arrangement of electrical heaters (ca. 100 kW). Transient and reversible operation between SOFC and SOEL are possible, also combined CO_2 and steam electrolysis operation (Co-SOEL). GALACTICA is partially automated, and the control system includes multiple control loops for power, in- and outlet temperatures, gas composition, current and reactant conversion, among others [30]. A set of thermocouples was installed within the LSM to measure the temperature at the inlet and outlet of each stack (the thermocouples for the air are depicted in Fig. 2c). Thermal transport phenomena such as radiation, conduction and convection cannot be neglected and therefore influence the estimation of the core temperature of the stacks.

GALACTICA consists of the following main components, as shown in the process flow diagram (PFD) in Fig. 2b:

1. Air supply unit: air blowers with inlet filters and mass flow measurement (details are given in the Appendix).
2. Gas supply unit: pressure regulators and electronic mass flow controllers for H_2, CO, CO_2, CH_4, and N_2. Pre-mixed Forming gas (95 Vol-% N_2/5 Vol-% H_2) is supplied with a mass flow meter with a manual needle valve, to ensure operation without power. Electronic mass flow controllers are used for controlling the composition and mass flow of the process gases.
3. Steam supply unit: The steam is generated by an electric steam generator with a maximum heating power of 45 kW. The volume flow of steam is measured with a swirl/vortex flow meter and regulated via an electrically controlled valve. The steam mass flow is calculated using external pressure- and temperature sensors. The feed water for the steam generator is purified by a reverse osmosis unit and continuously circulated through filter cartridges and an UV-disinfection unit.
4. Preheating Unit:

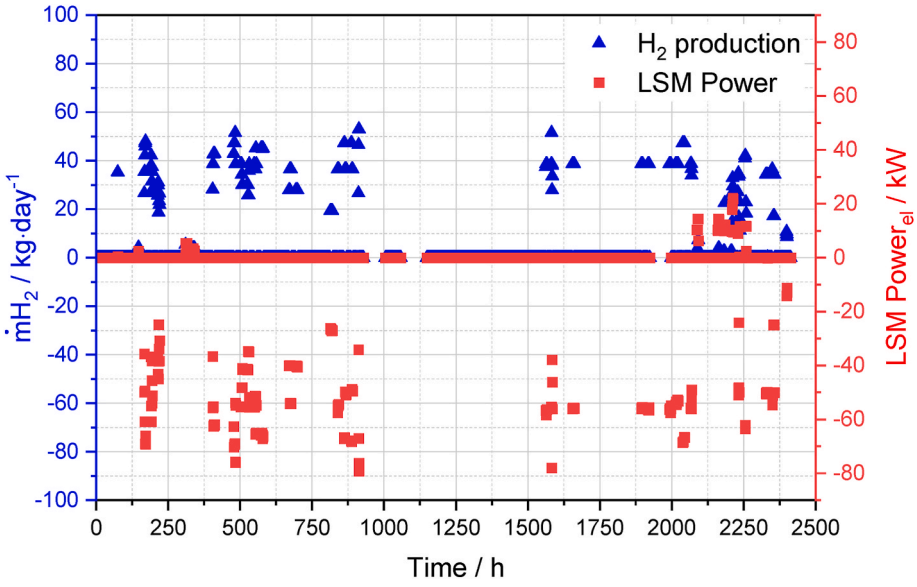

Fig. 3. Total testing time of the LSM showing the produced amount of hydrogen per day and electrical power through the whole campaign.

- Air heater: 40 kW electrical air preheater with a maximum air outlet temperature of 1050 °C.
- Gas heater: 2-stage gas heater setup, with 16 kW gas preheater (up to 300 °C) and a subsequent main heater, heating the gas-/steam mixture to a maximum temperature of 950 °C with a maximum power of 40 kW.

5. SOC Module: For this work, SolydEra's Large Stack Module (LSM) was integrated. However, other commercial SOC-Modules with electrolyte-supported cells have also been tested in GALACTICA.
6. Cooling and exhaust unit: gas-water and air-water heat exchangers are used to cool down the exhaust gas and air from the SOC-Module. The cooling water is supplied by the in-house cooling water circuit from DLR. More details are presented in the Appendix.
7. Gas analysis unit: a nondispersive infrared sensor analyzer from Rosemount with sensors for H_2, CO, CO_2 and CH_4 was used for measuring the dry gas composition of the gases in the exhaust of the SOC-Module.
8. Power electronics: GALACTICA is equipped with two sets of power electronics (with three or four channels) depending on the type of SOC-modules to be tested, i.e. on how the SOC stacks are internally arranged. In this work the used power electronics consisted of four bi-directional AC/DC converters that can individually be controlled, connected to the local 380 V AC power grid. Converters were limited to convert a maximum power of 30 kW, with a maximum of 200 V and a maximum current of 420 A. Details of the control and data acquisition are detailed on the Appendix.

2.4. *In situ characterizations techniques*

In situ characterization techniques, such as an online gas analysis of the product gases and electrochemical impedance spectroscopy (EIS) shed a glance on the system performance and on the identification and quantification of the area specific resistance (ASR), mainly the ohmic contribution. Electrochemical Impedance Spectroscopy (EIS) was performed in galvanostatic mode (1 A per stack, i.e. 0.05 mA cm^{-2}) close to open circuit voltage (OCV) with the workstation Zahner EL1000 in a frequency range from 50 mHz to 100 kHz. The amplitude of the current stimulus was 974 mA.

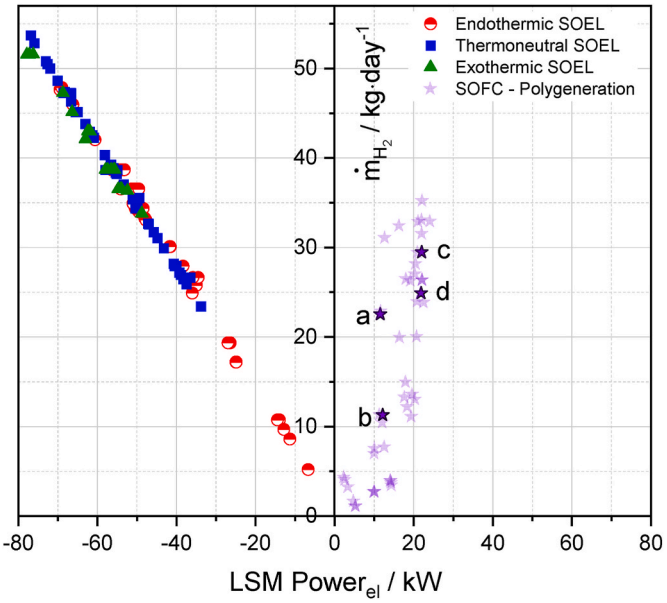

Fig. 4. Overview of operation points in exo-, endothermic and thermoneutral (isothermal) SOEL operation, as well as in SOFC – polygeneration mode (exothermic), depicting the daily net production of H_2 vs. the electrical power of the LSM. SOFC-polygeneration points of note: a) 11.5 kW_{el}, 22.5 kg H_2 day^{-1}, b) 12.1 kW_{el}, 11.3 kg H_2 day^{-1}, c) 22.0 kW_{el}, 29.5 kg H_2 day^{-1} and d) 22.6 kW_{el}, 24.9 kg H_2 day^{-1}.

3. Results and discussion

3.1. *Overview of the total testing time*

In the frame of this investigation, the LSM was operated for 2413 h (≈14 weeks), including hot operation, startup, shut-down, load operations, hot-standby for heater temperature amendments and general modifications, as well as during nights. Within this time, the LSM was tested for 307 h under load, from which 283 h were in SOEL mode and 24 h in SOFC mode. Throughout these experiments, relevant operating parameters such as the inlet and outlet temperatures of the air and gases were continuously monitored, while also analyzing their effect on the

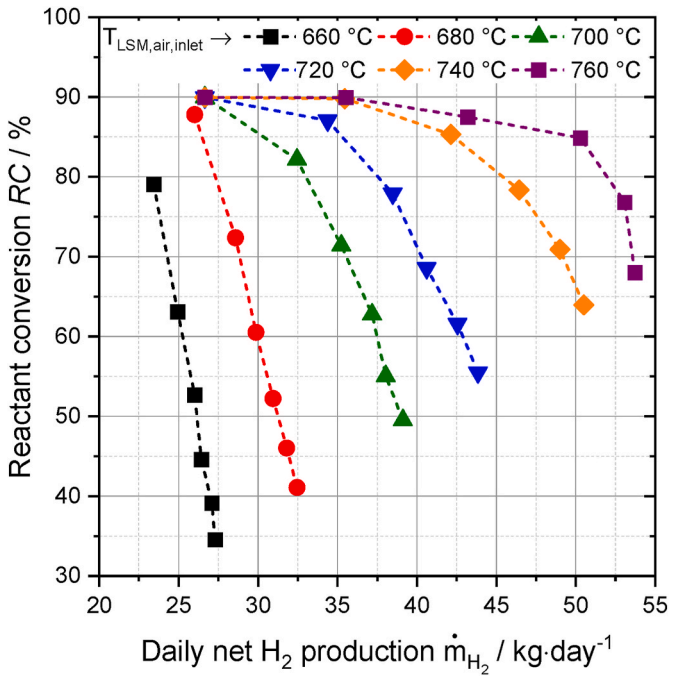

Fig. 5. Performance map of the LSM at thermoneutral (isothermal) SOEL operation with a 90 % H_2O – 10 % H_2 feed gas composition for different LSM air inlet temperatures at the module.

hydrogen production. The general and detailed results of these experiments are presented and discussed in the next section.

The full experimental campaign is depicted in Fig. 3, showing the electrical power input and hydrogen generation vs. the total testing time. Peak values of −75 kW in SOEL mode and 25 kW in SOFC mode were achieved. Details of the heating-up procedure and the dynamic polarization curves recorded at the beginning of the campaign are presented in the Appendix (Figure A1).

3.2. Endothermic, exothermic, isothermal and polygeneration operating points

Throughout the experimental campaign performed in this work, different load operation points were achieved. As shown in Fig. 4, the daily produced hydrogen is plotted as a function of power input/output, for which the operating modes were: SOEL (endothermic, exothermic and thermoneutral) and SOFC (exothermic). From this plot, it is possible to observe that the targeted daily hydrogen production of 53 kg was achieved in SOEL operation (exothermic and thermoneutral operation). In polygeneration mode about 29.5 kg day^{-1} were produced with a parallel power output of ca. 22 kW (c.f. point c) in Fig. 4). For the polygeneration mode it must be noted that the produced amount of hydrogen considers not only the pre-reforming reaction in eq. (1), but also the water gas shift reaction (WGS) in the downstream (c.f. Fig. 1) in eq. (2). These polygeneration results are detailed and depicted in section 3.6.

3.3. Performance map for isothermal SOEL operation

A performance map for the thermoneutral voltage operation in SOEL mode is shown in Fig. 5. Different isothermal operating points were evaluated with a constant fuel gas composition of 90 % H_2O – 10 % H_2, for which the LSM air inlet temperature in the range of 660–760 °C was considered. The thermoneutrality of each operating point was ensured by setting the voltage to 1.29 V per cell (ca. 77.4 V per stack). Hence, heat losses of the stacks and the LSM towards the environment were not considered. The reached current density for the thermoneutral operation was in the range of −0.34 and to −0.78 A cm^{-2} leading to an electrolysis input power between 34 and 77 kW. Fig. 5 shows the performance based on the daily net hydrogen production rate and the resulting reactant conversion (*RC*) for each operating point at a specific temperature. Within these operating modes, a daily net hydrogen production between 23 and 53 kg day^{-1} (11–25 Nm^3 h^{-1}) was achieved. The target daily production of 50 kg H_2 was successfully achieved for an average inlet temperature of ca. 740 °C (at *RC* of ca. 65 %) or even higher at 760 °C for *RCs* between 67 and 85 % (pink-colored area in Fig. 5). Nevertheless, at 660 and 680 °C the actual current densities reached for thermoneutral voltage were lower (with an average cell voltage of 1.29 V). Above 700 °C, the current supply had to be limited to not exceed a *RC* of 90 %.

3.4. SOEL stationary operating points

Among the SOEL experiments that were carried out, different stationary points were tested, as shown in Fig. 6. A set of seven operating points with a fuel mixture of 90 % H_2O – 10 % H_2 at a constant reactant conversion of 70 % and a module air inlet temperature of 720 °C were investigated. Along the 4 stacks of the LSM, the average cell voltage, the average temperatures of the stacks, as well as the air and fuel inlet temperatures, the electrical power of the LSM and the total ASR values of a steady state polarization curve are depicted on Fig. 6 d. The total ASR, considered also as a specific performance indicator, was calculated from eq. (3) [23] and eq. (4) (for SOEL, with the current density $J < 0$):

$$U_{op} = U_{ideal} - ASR_{Total} * J \quad \text{eq. (3)}$$

$$ASR_{Total} = \frac{U_{ideal} - U_{op}}{J} \quad \text{eq. (4)}$$

with the operational voltage U_{op} and the ideal voltage U_{ideal}. The ideal voltage was estimated with the Nernst Potential for the case of an SOEL cell as in eq. (5), considering $z = 2\ e^-$, the $\overline{y_i}$ as the linear averaged gas composition between in- and outlet of the stack and assuming a linear conversion over the length of the electrochemically active cell area.

$$U_{ideal,SOEL} = -\frac{\Delta G_r^0}{zF} + \frac{RT}{zF} * \ln\left(\frac{\overline{y}_{H_2} * \overline{y}_{O_2}^{\frac{1}{2}}}{\overline{y}_{H_2O}}\right) + \frac{RT}{zF} * ln\left(\frac{p}{p_o}\right)^{\frac{1}{2}} \quad \text{eq. (5)}$$

Therefore, the ASR_{Total} calculated with eq. (4) considers a conversion correction, allowing to compare different operating points with different experimental parameters (i.e. temperature, current density, reactant conversion) [31].

As observed in Fig. 6a, the average cell voltages of all stacks are similar throughout the whole operating range, which is also consistent to the homogeneous temperature profile of the stacks either for endothermic (below 1.29 V) or for exothermic mode (above 1.29 V per cell). Such homogeneous behavior among the stacks could be related to a homogeneous feed gas distribution inside the LSM, leading also to a similar electrochemical performance of each stack.

The isothermal operating point of the LSM was identified at an average stack temperature of ca. 720 °C with an average cell voltage of 1.31 V for these experimental conditions, corresponding to a heat loss of the whole LSM of approximately of 1.3 kW. The most SOEL exothermic point was identified at a current density of −0.75 A cm^{-2}, which corresponds to an input of electrical power of −75 kW of the LSM.

Furthermore, aiming at developing an expression for the total *ASR* as a function of the air temperature, the expression in eq. (6) was used for calculating the $ASR_{Total,iV}$ from the polarization curves in Fig. 6d, for which *R* represents the universal gas constant, the independent variable is the operating temperature *T* (in K) at thermoneutral condition, T_o as the reference temperature at 1073.15 K and E_{a_1} as the apparent activation energy of this thermal dependency of the total ASR. This estimation will be discussed and compared with the *ASR* from EIS in section 3.5.

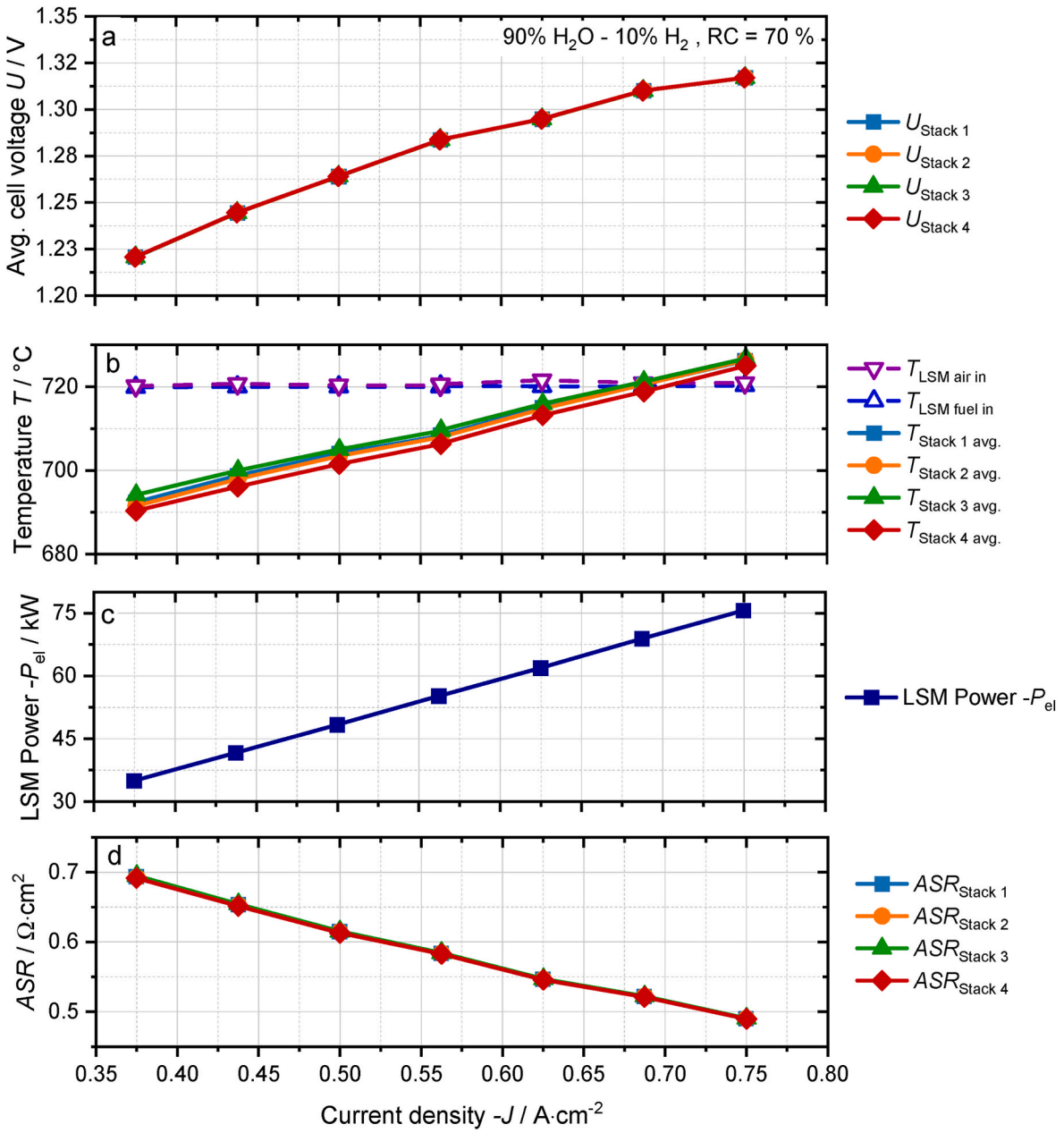

Fig. 6. (a): Steady state *U*(*i*)-curve for electrolysis operation with a constant reactant conversion *RC* of 70 % at an average inlet temperature of ca. 720 °C. (b) Stack average temperatures, as well as the module inlet air and fuel temperatures. (c): Electrical power consumed by the LSM at the tested stationary operation. (d): Calculated total *ASR* as a function of the current density *J* by using eq. (4).

$$ASR_{\text{Total},iV} = ASR_{o} * \exp\left(\frac{E_{a_1}}{R} * \left(\frac{1}{T} - \frac{1}{T_o}\right)\right) \quad \text{eq. (6)}$$

3.5. ASR assessment

Two different approaches were followed for developing an expression of the *ASR* as a function of the air temperature, considering (i) the outlet temperature of the stacks and (ii) the average value between inlet and outlet air temperatures. These approaches were considered for the *ASR* estimation via EIS and steady state polarization curves, as following.

3.5.1. Ohmic ASR analysis via EIS

EIS measurements close to OCV conditions of Stack 1 are shown in Fig. 7 for different average air temperatures: 740 °C, 710 °C, 705 °C, 680 °C, 665 °C and 650 °C. The Nyquist plot (Fig. 7 a) depicts two semicircle-like features for all temperatures. Closer observation of the real impedance (Z_{re}) axis intercepts depicts the increment of the ohmic resistance upon temperature decrement, which is consistent to the ionic conductivity behavior on ceramic oxide-based electrolytes.

Fig. 7b shows the imaginary contribution of the Nyquist plot for Stack 1, as this set of data is representative for the other stacks. At high and mid characteristic frequencies, charge transfer reactions on the fuel and electrode take place. However, due to the cumulated area of the cells along the stack, it is difficult to deconvolute the spectra to identify the different electrochemical reactions. At low frequencies (ca. 0.1 Hz), it is possible to observe a thermal-activated gas conversion process, where the resistance decreased with decreasing temperature [32]. Nevertheless, identification on the different losses within the cells is limited with these spectra due to high gas conversion losses during the measurement (60 % H_2 – 40 % N_2), as well as for the cumulative area of

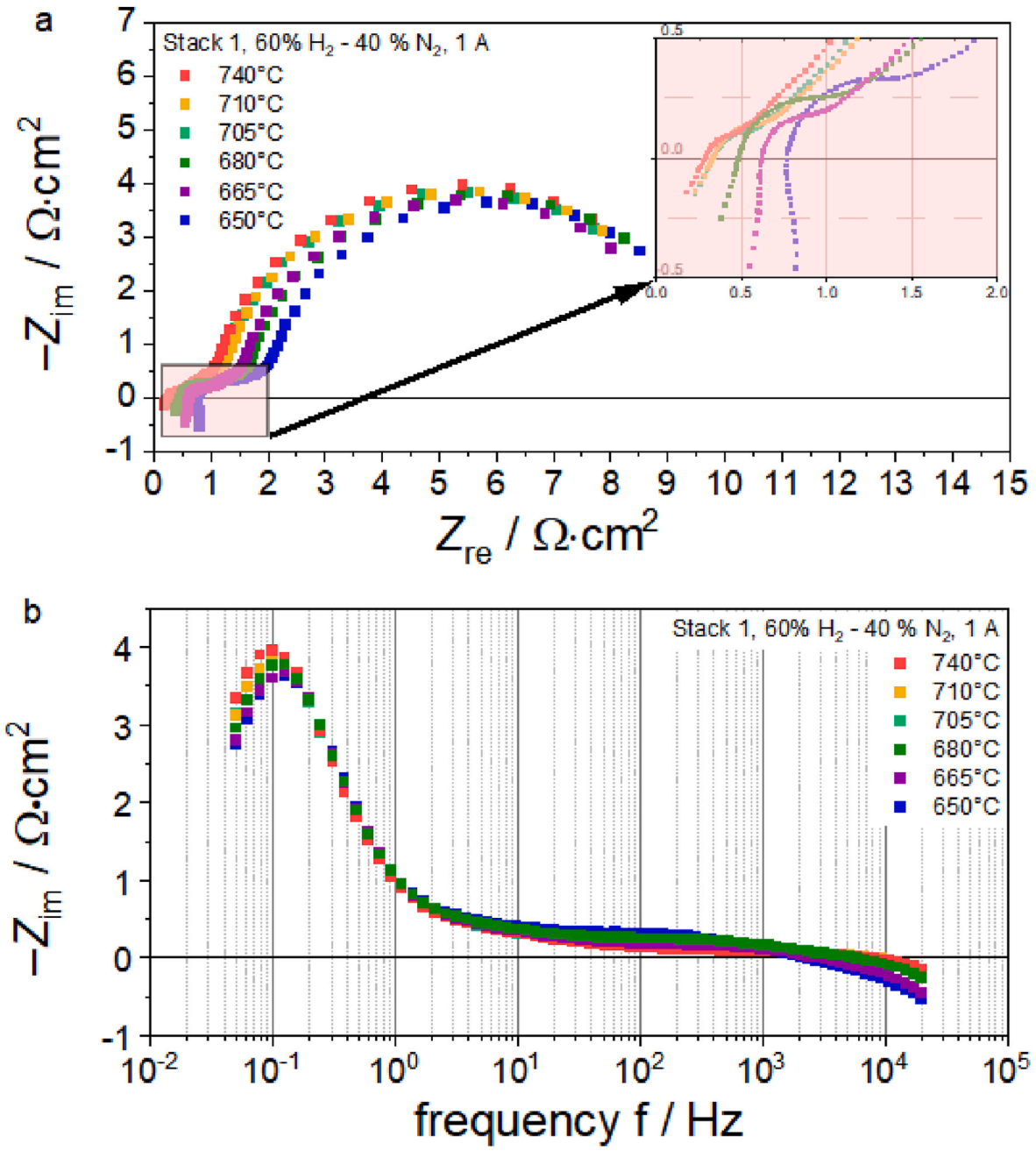

Fig. 7. EIS spectra recorded close at OCV for Stack 1 at 740 °C, 710 °C, 705 °C, 680 °C, 665 °C and 650 °C: (a) Nyquist and (b) imaginary impedance plots for the fuel gas mixture of 60 % H_2−40 % N_2.

Table 1
Fitting parameters for the ohmic *ASR* calculation using eq. (7) considering the measured average air temperature and the outlet air temperature in K. The exponential fits were performed with EIS data from the four stacks.

Parameter	$ASR_{\text{ohmic,EIS}} = f(T_{average\,air})$	$ASR_{\text{ohmic,EIS}} = f(T_{out\,air})$
ASR_o ($\Omega\,cm^2$)	0.2425 ± 0.0135	0.2436 ± 0.0193
B	0.0037 ± 0.0015	0.0027 ± 0.0016
E_{a_2} ($J\,mol^{-1}$)	273582 ± 20815	283055 ± 30959
R^2 (COD)	0.9893	0.9755

the cells along the stack. Also, the gas diffusion losses cannot be neglected in fuel electrode-supported architectures. However, electrochemical characterization via EIS on large-stack-modules could shed new insights on the thermal dependency of the ohmic contribution and hence predict the overall performance of the LSM.

The temperature dependence of the $ASR_{ohmic,EIS}$ was estimated from the EIS measurements in all four stacks of the LSM. With the obtained values of the ohmic resistance, it was possible to estimate the temperature dependence of the ohmic area specific resistance $ASR_{\text{ohmic,EIS}}$ with the Arrhenius-type expression in eq. (7), for which T is considered in K:

$$ASR_{\text{ohmic,EIS}} = ASR_o + B^{*}\exp\left(\frac{E_{a_2}}{R}*\left(\frac{1}{T}-\frac{1}{T_o}\right)\right) \quad \text{eq. (7)}$$

Table 1 presents the fit values for ASR_o, B and the apparent activation energy E_{a_2} of the thermal dependency of the ohmic ASR considering the average air temperature and the outlet air temperature, with their corresponding coefficient of determination (COD) R^2. These data are plotted in Fig. 8.

This temperature dependency is also influenced by the measurement

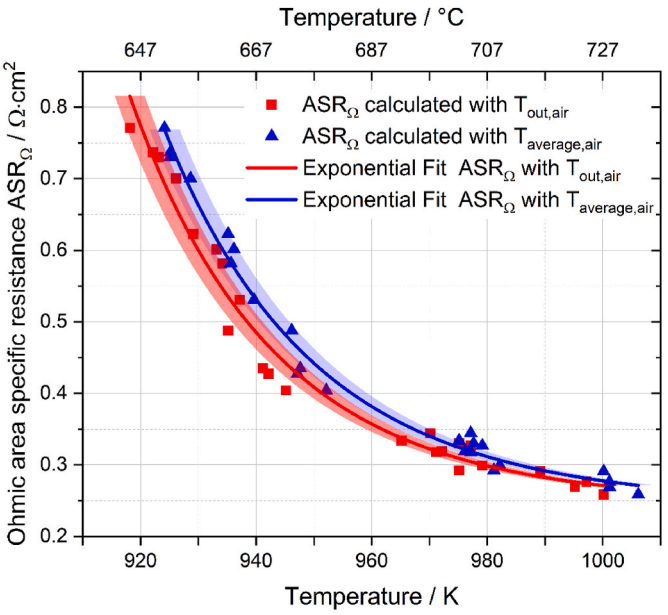

Fig. 8. Temperature dependency of the ohmic ASR considering the average air temperature (blue data) and the outlet air temperature (red data). (For interpretation of the references to color in this figure legend, the reader is referred to the Web version of this article.)

Table 2
Fitting parameters for the total *ASR* calculation using eq. (6), considering the average air temperature and the outlet air temperature. The exponential fits were performed with steady state polarization curves from Fig. 6d.

Parameter	$ASR_{TotaliV} = f(T_{average,air})$	$ASR_{TotaliV} = f(T_{out,air})$
ASR_o ($\Omega\ cm^2$)	0.2515 ± 0.0781	0.3527 ± 0.0399
E_{a_1} ($J\ mol^{-1}$)	80674 ± 1871	45340 ± 680
R^2 (COD)	0.9841	0.9933

uncertainties, which were ±0.4 % (DIN EN 60584 for thermocouples type K, class 1). The effect of these uncertainties is depicted via the shaded regions in Fig. 8.

From the plots in Fig. 8, it is possible to observe that there is a slight difference of the calculated $ASR_{ohmic,EIS}$ at low temperatures, i.e. at 650 °C until ca. 700 °C. For instance, at 650 °C the data that consider the outlet air temperature varies between 0.7 and 0.8 Ω cm^2. On the contrary, taking the average air temperature data, a lower dispersion of the ohmic *ASR* is observable. For higher temperatures, i.e. from 725 °C, the difference among the two data sets is negligible, reaching $ASR_{ohmic,EIS}$ values of ca. 0.25 Ω cm^2, which is in agreement with the values reported by Riedel et al. on fuel-electrode-supported-cell stacks tested in SOEL operation at 1.4 bar (80 % H_2O – 20 % H_2) [33]. However, for the herein investigated LSM, it is possible to assume that the $ASR_{ohmic,EIS}$ temperature dependency could be described with the average between the inlet and outlet air temperature measured during the experimental campaign.

3.5.2. Total ASR estimation by polarization curves in SOEL stationary operation

Based on the steady state experimental results in isothermal SOEL operation shown in Fig. 6d, the total *ASR* from the polarization curve ($ASR_{TotaliV}$) was estimated with eq. (4) at thermoneutral conditions. Table 2 presents the fit values for ASR_o and E_{a_1} considering the average air temperature and the outlet air temperature with their corresponding (COD) R^2.

Contrary to the estimated $ASR_{ohmic,EIS}$, the $ASR_{TotaliV}$ temperature dependency not only represents the ohmic losses η_{ohmic} influence on the *ASR* of the cells within the LSM, but also it considers the different

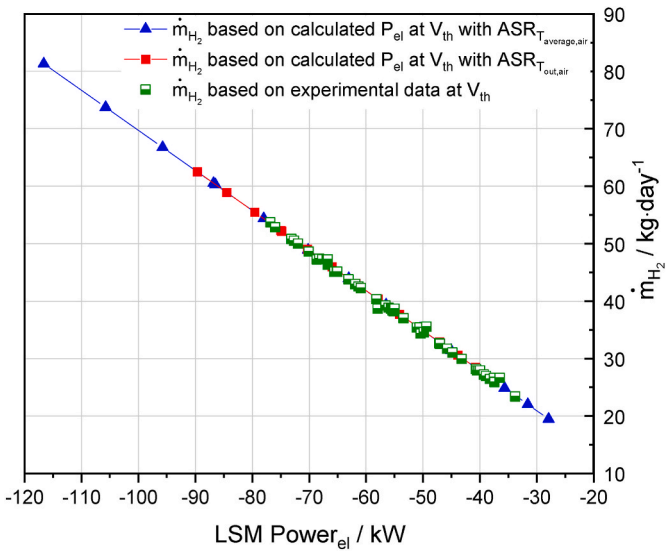

Fig. 9. The daily net hydrogen production calculated from eq. (12) is plotted against the consumed electrical power of the LSM, considering the average air temperature (in blue) and the outlet air temperature (in red). The experimental data are depicted in green. (For interpretation of the references to color in this figure legend, the reader is referred to the Web version of this article.)

contribution to the *ASR* from the activation η_{act} and gas conversion losses η_{conc}, as eqs. (8) and (9) suggest:

$$ASR_{total} = \frac{|\eta_{act} + \eta_{ohmic} + \eta_{conc}|}{J} \quad \text{eq. (8)}$$

$$ASR_{Total} = (ASR_{act}) + (ASR_{ohmic}) + (ASR_{conc}) \quad \text{eq. (9)}$$

Therefore, it is possible to estimate the LSM electrical power consumption at thermoneutral operation $P_{el_{th}}$ as a function of the ASR_{Total}, as explained in eqs. (10)–(12):

$$P_{el_{th}} = U_{th} * A\left(\frac{U_{ideal} - U_{th}}{ASR_{Total_{iV}}}\right) \quad \text{eq. (10)}$$

$$P_{el_{th}} = U_{th} * \frac{A}{ASR_{Total_{iV}}}(U_{ideal} - U_{th}) \quad \text{eq. (11)}$$

$$P_{el_{th}} = U_{th} * \frac{A}{ASR_{Total_{iV}}} * \left[-\frac{\Delta G_r^0}{zF} + \frac{RT_{th}}{zF} * \ln\left(\frac{\bar{y}_{H_2} * \bar{y}_{O_2}^{\frac{1}{2}}}{\bar{y}_{H_2O}}\right) - U_{th} \right] \quad \text{eq. (12)}$$

For which U_{th} corresponds to the thermoneutral voltage of the cells at the tested conditions, *A* the total active area of the RUs within the LSM, and $\bar{y}_i$ the actual molar fractions of the reacting species *i* in equilibrium (corrected with the *RC*). Nevertheless, the daily net production of hydrogen $\dot{m}_{H2}$ is one of the most relevant performance indicators of a SOEL system. For this reason, a calculation of $\dot{m}_{H2}$ with the $P_{el_{th}}$ from eq. (12) (calculated from $ASR_{TotaliV}$) is explained as following:

$$I_{th} = \frac{P_{el_{th}}}{U_{th} * N_{RUs} * N_{Towers}} \quad \text{eq. (13)}$$

$$\dot{m}_{H_2} = \frac{P_{el_{th}}}{U_{th} * zF * PM_{H_2}} \quad \text{eq. (14)}$$

With eq. (14), the daily net production of hydrogen vs. the electrical power of the LSM at thermoneutral conditions is depicted in Fig. 9 (right axis), which is in agreement with the experimental data (green dots), also shown in Fig. 4, despite the difference between the $ASR_{TotaliV}$ approaches.

The difference between the $ASR_{ohmic,EIS}$ and the $ASR_{TotaliV}$ (considering only the average air temperature), is explained by eq. (9). Besides

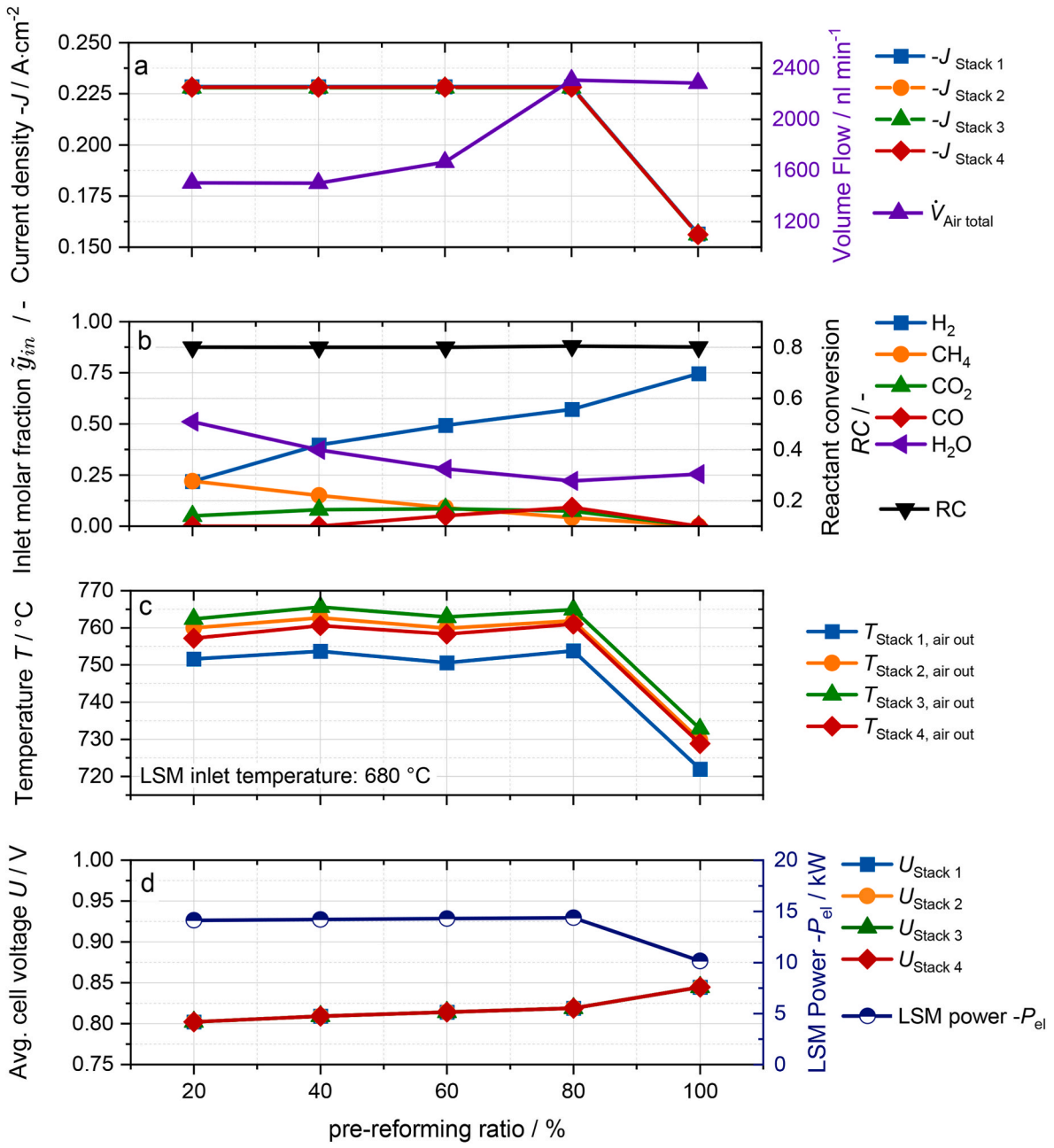

Fig. 10. Investigation of the influence of the pre-reforming ratio between 20 % and 100 % on the LSM performance. (a): Current density and total air flow. (b): Inlet molar compositions and reactant conversion. (c): Temperature profiles of the outlet temperature of the stacks. (d): Stack voltages and LSM power.

the ohmic contribution of the electrolyte, the total *ASR* also includes the activation and the gas conversion losses. It is important to note that the EIS measurements were performed close to OCV conditions with a fuel gas composition that leads to high conversion losses, as observed in Fig. 7b at low frequencies (≈ 0.1 Hz) for the different tested temperatures. These values should be carefully compared with the ASR_{TotaliV}, since the polarization curves were performed in SOEL thermoneutral operation and the EIS measurements with a slight anodic bias of 1 A.

Beyond the scope of this work, a more accurate estimation of the ASR_{Total} could consider the EIS measurements not only close to OCV conditions, but also recorded at relevant current densities for SOEL operation. With this, the low frequency impedance values could serve to estimate the gas losses contribution at a relevant operating condition. Complementary, an expression of the activation losses as a function of the thermoneutral current density would give an insight of the different losses within the air and fuel electrodes of the cells inside the LSM, such as suggested by Njodzefon et al. [34]. It is recommended to use the same gas mixture for both EIS and polarization curve measurements, preferably where the gas conversion losses are reduced for SOEL operation [34].

3.6. SOFC and polygeneration stationary operating points

With the aim to emulate the SOFC operation with a pre-reformer, different stationary operating points were evaluated for five pre-reforming ratios (20 %, 40 %, 60 %, 80 % and 100 %), as depicted in Fig. 10. For the feed of the pre-reformer a mixture of steam and methane was assumed with a steam to carbon ratio (S/C) of 2.3. The pre-reforming ratio is defined by the amount of methane that is converted in the reformer. Thus, e.g. at a pre-reforming ratio of 20 %, 80 % of the CH_4 is converted in the LSM, while the rest is already converted to H_2, CO and CO_2 in the reformer. Equilibrium calculations at the reformer

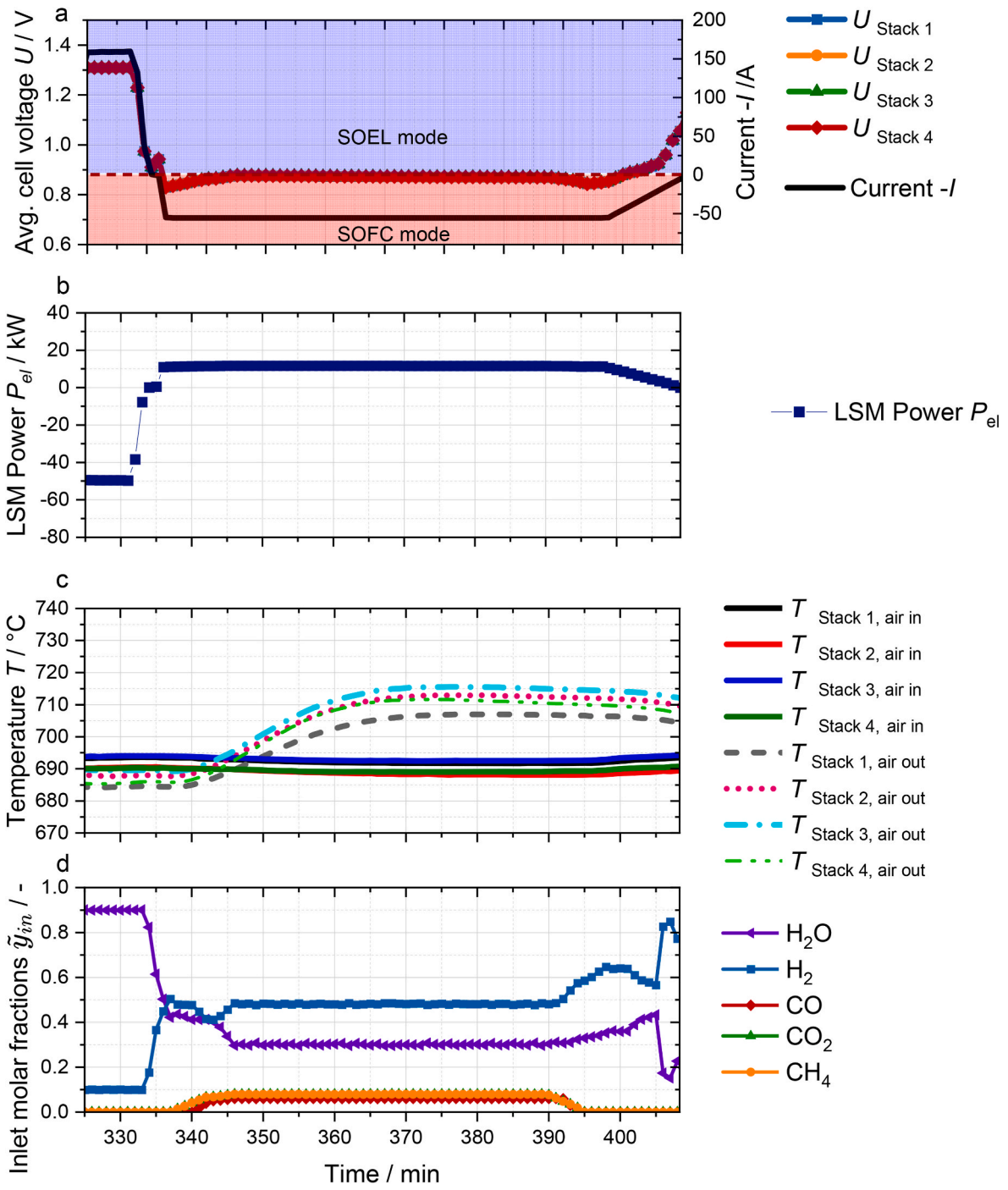

Fig. 11. (a): Switch procedure from −50 kW SOEL operation to SOFC polygeneration mode. (b): Consumed and produced electrical power of the LSM. (c): Temperature profiles along the stacks of the air inlet and outlet temperature. (d): Inlet molar fractions.

were used to obtain the corresponding molar concentrations for each of the evaluated points at the SOFC feed. It should be mentioned that during the experimental campaign, the molar concentrations had to be changed for the 100 % pre-reforming point by replacing CO with H_2. The composition was changed since this operation point considers the highest CO flow at the inlet of the SOFC, exceeding the maximum flow capabilities of the test rig, and thus compromising the safety of the experiment. Furthermore, the experiments for pre-reforming ratios of 20–80 % were carried out with a constant power output of 15 kW while the operation point with 100 % pre-reforming was carried out with a lower power output of 10 kW. This was done in order to avoid an overheating of the stacks, since the air flow for cooling purposes was limited to 2300 nl min^{-1}. Fig. 10 shows that the outlet temperature of the stacks presented similar behavior for the pre-reforming ratios between 20 and 80 % due to the adaption of the cooling air flow. These results are not only presenting the direct H_2 production within the LSM via steam methane reforming (c.f. eq. (1)), but also including the H_2 by the water gas shift reaction (WGS – eq. (2)), assuming that one methane molecule results in four hydrogen molecules.

3.7. Switching from SOEL to SOFC and polygeneration operating modes

The procedure of switching between operating modes was performed from SOEL, transitioning to SOFC and further to polygeneration mode.

Table 3
Air flow, gas compositions, current and reactant conversion during steady state polygeneration operation at an inlet temperature of 680 °C.

LSM inlet temperature	Air flow	H_2	H_2O	CO_2	CO	N_2	CH_4	*I*	*RC*
°C	nl min^{-1}	mol-%	mol-%	mol-%	mol-%	mol-%	mol-%	A	%
680	2000	41	22	7	5	18	7	55.5	33

As shown in Fig. 11, this procedure was performed under 30 min, starting near to thermoneutral operation (ca. isothermal) in electrolysis with a power of −50 kW, for which the voltage per stack was kept for ca. 10 min at 82 V, i.e. 1.37 V per RU, with a fuel gas mixture of 90 % H_2O – 10 % H_2. Then, the flowrate of steam was decreased while increasing the hydrogen flow for 5 min. In parallel, the current was also decreased to zero. Once OCV conditions were reached, it was possible to switch to SOFC-polygeneration mode by increasing the current and reaching a power output of 15 kW with a fuel gas mixture of ca. 55 % H_2O – 45 % H_2. In the following 5 min, CH_4, CO and CO_2 flowrates were added with the aim to avoid overheating of the stacks due to the exothermic operation, achieving steady state operation with the conditions on Table 3. As depicted in Fig. 11, the LSM reached a stationary state for 1 h in exothermic operation (for which the stack temperatures increased up to ca. 715 °C) and the power output was kept at 15 kW. During the procedure, the absolute temperature difference recorded between stack air inlet and outlet remained within the range 9.2 ± 3.9 K in SOEL to 21.3 ± 6.4 K in polygeneration, thus fulfilling the manufacturer maximum temperature difference specification, as well as stack temperature homogeneity.

With this switching procedure, it is possible to assume that such transient operation does not lead to risks for the lifetime of the LSM at the herein tested conditions of current and gas mixtures, since the temperature profile along the stacks was homogeneous and the average voltage values per RU were kept within safety limits. In particular, the undervoltage and short circuit protection values that correspond to an average RU voltage of 0.74 V and 0.67 V respectively, were not reached.

4. Conclusion

Within the frame of this investigation, it was possible to demonstrate the reversible operation of a 25 kW_{el} LSM from SolydEra for a total testing time of ca. 2413 h, reaching peak values of 25 kW in SOFC mode and ca. −75 kW in SOEL operation. The LSM showed homogeneous temperature and voltage profiles of all four stacks during the different conducted experiments. Steady state tests at different operation conditions of temperature, reactant conversion, current densities and fuel gas compositions showed that the production rates are in line with the expectations of the SWITCH prototype:

(i) The production capacity required for the SWITCH system was met in SOEL operation with a reactant conversion of 90 % (fuel gas mixture of 90 % H_2O – 10 % H_2) in a temperature range between 680 °C and 760 °C, achieving a daily net production of hydrogen between 25 and 53 kg day^{-1}. These results allowed to develop a performance map of the reactant conversion and the daily net hydrogen production for different operating temperatures.
(ii) For the SOFC-polygeneration mode, a power output between 11 and 22 kW with about 12 and 30 kg day^{-1} of hydrogen production was achieved. Within these experiments, a variation of the pre-reforming ratio between 20 and 100 % was conducted. Despite the endothermic nature of the CH_4 reforming, the LSM was operated in exothermic conditions since the outlet temperature of all stacks was higher than the inlet temperatures by more than 47 K.
(iii) The switching between SOEL and SOFC operation modes was successfully performed under 30 min, demonstrating stable operation and homogenous temperatures, voltage and gas compositions (switching within less time was also possible, but due to the thermal inertia of the LSM the shortest time to achieve steady operation was 30 min).

Regarding the temperature dependency of the *ASR*, steady state data of polarization curves on the endothermic, thermoneutral and exothermic SOEL operation regimes allowed to quantify the total *ASR* of the LSM at relevant current densities, from −0.35 to −0.75 A cm^{-2}. The ohmic *ASR* was estimated by electrochemical impedance spectroscopy (EIS) of each stack close to OCV conditions. Even though the ohmic *ASR* estimation is complementary to the total *ASR*, the latter served to estimate different performance indicators (i.e. the net hydrogen production), since the total *ASR* estimation from the polarization curves consider also the contribution of the activation and gas conversion losses within the LSM.

The daily net production of hydrogen is an important performance indicator since it is correlated to the electrical power consumption of the LSM. Furthermore, the SWITCH concept is to produce a secured amount of hydrogen in both its SOEL and polygeneration modes, which was experimentally estimated within this research. At isothermal SOEL operation, i.e. close to thermoneutral voltage, it was demonstrated that the estimation of the required electrolysis power as a function of the total *ASR* serves as ground base for predicting the power consumption for system scale-up approaches, that go beyond the technical limitations of lab-scale test environments.

In general, the results herein presented could shed more light to other researchers and technology providers on the operational advantages of performing switching procedures in SOC systems at relevant industrial scales. Furthermore, control strategies for the transient operation of these systems should be thoroughly investigated, with the motivation to mitigate the risk of deteriorating the LSM lifetime with thermo-mechanical stress conditions that could arise. Therefore, the experimental results shown in this investigation would be the basis for the parametrization of transient simulation models that consider spatial and temporal temperature gradients, different gas compositions and part- and full-load operation, e.g. by switching between hot standby conditions and isothermal operation of the individual stacks, or even of modules (at the MW scale) [35]; conditions that are beyond the technical limitations of scientific experimental investigations. Because of such limitations, the development of simulation frameworks that allow to investigate critical operation conditions on large SOC systems is a key feature for the further improvement and deployment of these systems. In the frame of this investigation a detailed analysis of modelling results will be published [21,36].

Declaration of competing interest

The authors declare that they have no known competing financial interests or personal relationships that could have appeared to influence the work reported in this paper.

Acknowledgement

The authors would like to highlight and acknowledge the close collaboration with SolydEra in the execution and design of the experiments. Many thanks for the open-minded discussions and the very valuable contributions in this cooperation. In addition, the authors

emphasize that the work for this paper was funded by the project SWITCH which received funding from the Fuel Cells and Hydrogen 2 Joint Undertaking (now Clean Hydrogen Partnership) under Grant Agreement No 875148. This Joint Undertaking receives support from the European Union's Horizon 2020 research and innovation programme, Hydrogen Europe and Hydrogen Europe Research.

Appendix A. Supplementary data

Supplementary data to this article can be found online at https://doi.org/10.1016/j.ijhydene.2024.01.346.

References

[1] IEA. Net Zero by 2050. Paris: International Energy Agency; 2021. https://wwwieaorg/reports/net-zero-by-2050.
[2] A hydrogen strategy for a climate-neutral Europe. European Comission; 2020.
[3] van Wijk PDA, Chatzimarkakis J. Green hydrogen for a European green deal A 2x40 GW initiative. Hydrogen Europe.
[4] Hydrogen roadmap Europe: a sustainable pathway for the European energy transition. Fuel Cells Hydrogen 2.
[5] Hauch A, Kungas R, Blennow P, Hansen AB, Hansen JB, Mathiesen BV, et al. Recent advances in solid oxide cell technology for electrolysis. Science 2020:370.
[6] Tamburrano G, Pumiglia D, Monforti Ferrario A, Santoni F, Borello D. Analysis of the performances of a solid oxide fuel cell fed by biogas in different plant configurations: an integrated experimental and simulative approach. Int J Hydrogen Energy 2024;52:745–60.
[7] Hauch A, Ploner A, Pylypko S, Cubizolles G, Mougin J. Solid oxide cells and stacks for reversible operation at high current densities. ECS Meet Abstr 2020; MA2020–01:1505.
[8] Morales-Zapata MA, Larrea A, Laguna-Bercero MA. Reversible operation performance of microtubular solid oxide cells with a nickelate-based oxygen electrode. Int J Hydrogen Energy 2020;45:5535–42.
[9] Lang M, Lee Y-s, Lee I-s, Szabo P, Hong J, Cho J, et al. Analysis of degradation phenomena of SOC stacks operated in reversible SOFC/SOEC cycling mode. ECS Trans 2023;111:181.
[10] Peters R, Frank M, Tiedemann W, Hoven I, Deja R, Kruse N, et al. Long-term experience with a 5/15kW-class reversible solid oxide cell system. J Electrochem Soc 2021;168:014508.
[11] Königshofer B, Boškoski P, Nusev G, Koroschetz M, Hochfellner M, Schwaiger M, et al. Performance assessment and evaluation of SOC stacks designed for application in a reversible operated 150 kW rSOC power plant. Appl Energy 2021; 283:116372.
[12] Ploner A, Hauch A, Pylypko S, Di Iorio S, Cubizolles G, Mougin J. Optimization of solid oxide cells and stacks for reversible operation. ECS Trans 2019;91:2517.
[13] Aicart J, Wuillemin Z, Gervasoni B, Reynaud D, Waeber F, Beetschen C, et al. Performance evaluation of a 4-stack solid oxide module in electrolysis mode. Int J Hydrogen Energy 2022;47:3568–79.
[14] Peters R, Blum L, Deja R, Hoven I, Tiedemann W, Küpper S, et al. Operation experience with a 20 kW SOFC system. Fuel Cell 2014;14:489–99.
[15] Tomberg M, Heddrich MP, Metten M, Ansar SA, Friedrich KA. Operation of a solid oxide fuel cell reactor with multiple stacks in a pressured system with fuel gas recirculation. Energy Technol 2022;10:2101075.
[16] Reytier M, Di Iorio S, Chatroux A, Petitjean M, Cren J, De Saint Jean M, et al. Stack performances in high temperature steam electrolysis and co-electrolysis. Int J Hydrogen Energy 2015;40:11370–7.
[17] Reytier M, Cren J, Petitjean M, Chatroux A, Gousseau G, Di Iorio S, et al. Development of a cost-efficient and performing high temperature steam electrolysis stack. ECS Trans 2013;57:3151.
[18] Mougin J, Chatroux A, Couturier K, Petitjean M, Reytier M, Gousseau G, et al. High temperature steam electrolysis stack with enhanced performance and durability. Energy Proc 2012;29:445–54.
[19] Mougin J, Di Iorio S, Chatroux A, Donnier-Marechal T, Palcoux G, Petitjean M, et al. Development of a solid oxide electrolysis stack able to operate at high steam conversion rate and integration into a SOE system. ECS Trans 2017;78:3065.
[20] Santhanam S, Heddrich MP, Riedel M, Friedrich KA. Theoretical and experimental study of Reversible Solid Oxide Cell (r-SOC) systems for energy storage. Energy 2017;141:202–14.
[21] Srikanth S, Heddrich MP, Gupta S, Friedrich KA. Transient reversible solid oxide cell reactor operation – experimentally validated modeling and analysis. Appl Energy 2018;232:473–88.
[22] Nuggehalli Sampathkumar S, Aubin P, Couturier K, Sun X, Sudireddy BR, Diethelm S, et al. Degradation study of a reversible solid oxide cell (rSOC) short stack using distribution of relaxation times (DRT) analysis. Int J Hydrogen Energy 2022;47:10175–93.
[23] Amaya-Dueñas DM, Riegraf M, Nenning A, Opitz AK, Costa R, Friedrich KA. Operational aspects of a perovskite chromite-based fuel electrode in solid oxide electrolysis cells (SOEC). ACS Appl Energy Mater 2022;5(7):8143–56.
[24] Rinaldi G, Diethelm S, Oveisi E, Burdet P, Van herle J, Montinaro D, et al. Post-test analysis on a solid oxide cell stack operated for 10,700 hours in steam electrolysis mode. Fuel Cell 2017;17:541–9.
[25] Lang M, Raab S, Lemcke MS, Bohn C, Pysik M. Long-term behavior of a solid oxide electrolyzer (SOEC) stack. Fuel Cell 2020;20:690–700.
[26] Bolognese M, Testi M, De Bortoli L, Bartali R, Crema L. Experimental validation of a dynamic modelling of a reversible solid oxide cells (rSOCs). E3S Web Conf 2022; 334:01003.
[27] Amaya-Dueñas D-M, Riedel M, Riegraf M, Costa R, Friedrich KA. High temperature Co-electrolysis for power-to-X. Chem Ing Tech 2020;92:45–52.
[28] Fu Q, Mabilat C, Zahid M, Brisse A, Gautier L. Syngas production via high-temperature steam/CO2 co-electrolysis: an economic assessment. Energy Environ Sci 2010;3:1382–97.
[29] Pérez-Fortes M, Mian A, Srikanth S, Wang L, Diethelm S, Varkaraki E, et al. Design of a pilot SOFC system for the combined production of hydrogen and electricity under refueling station requirements. Fuel Cell 2019;19:389–407.
[30] Thermodynamics GACD-IoE. GALACTICA-Experimental environment for SOC reactors with multiple stacks. https://wwwdlrde/tt/en/desktopdefaultaspx/tabid-18796/30129_read-80921/2022.
[31] Riedel M, Heddrich MP, Friedrich KA. Analysis of pressurized operation of 10 layer solid oxide electrolysis stacks. Int J Hydrogen Energy 2019;44:4570–81.
[32] Bessler WGG. Stefan gas concentration impedance of solid oxide fuel cell anodes II. Channel geometry. J Electrochem Soc 2007;154:B548–59.
[33] Riedel M, Heddrich MP, Ansar A, Fang Q, Blum L, Friedrich KA. Pressurized operation of solid oxide electrolysis stacks: an experimental comparison of the performance of 10-layer stacks with fuel electrode and electrolyte supported cell concepts. J Power Sources 2020;475:228682.
[34] Njodzefon JC, Klotz D, Kromp A, Weber A, Ivers-Tiffée E. Electrochemical modeling of the current-voltage characteristics of an SOFC in fuel cell and electrolyzer operation modes. J Electrochem Soc 2013;160:F313.
[35] Tomberg M, Heddrich MP, Ansar SA, Friedrich KA. Operation strategies for a flexible megawatt scale electrolysis system for synthesis gas and hydrogen production with direct air capture of carbon dioxide. Sustainable Energy & Fuels; 2023.
[36] Tomberg M, Heddrich MP, Sedeqi F, Ullmer D, Ansar SA, Friedrich KA. A new approach to modeling solid oxide cell reactors with multiple stacks for process system simulation. J Electrochem Soc 2022;169:054530.